Generation of intense pulsed electric fields in a large volume of water verified using Kerr effect diagnostics

Generation of Intense Pulsed Electric Fields in a Large Volume of Water Verified Using Kerr Effect Diagnostics

Matthew Woodyard, *Graduate Student Member, IEEE*, Bucur M. Novac, *Senior Member, IEEE*, Peter Senior, *Member, IEEE*, and Jessica M. Stobbs, *Graduate Student Member, IEEE*

***Abstract*— A pulsed power system for generating intense pulsed electric fields (PEFs) in a very large volume of water was designed, manufactured, and tested as a first step toward the proof-of-principle demonstration of a novel noninvasive prepacked food processing operation. The MV-class system described in this article is based on the Tesla transformer technology and is capable of producing PEFs of 100 kV/cm in water, in a volume approaching 1 L. The electric field distribution in the processing water tank was obtained using an electrostatic solver, benchmarked using a Kerr effect arrangement. This article presents the most important experimental data, followed by a detailed electric field analysis and suggestions for the way ahead.**

***Index Terms*— Kerr effect, pulsed electric fields (PEFs), pulsed power technology, Tesla transformer.**

I. Introduction

PULSED electric field (PEF) food processing is a well-established technology. In most situations, a number of metallic electrode pairs are energized using pulsed power generators to produce intense PEFs in an industrial liquid food (sometimes termed "pumpable" food), for producing the required level of sterilization. As the pairs of electrodes between which the PEF is generated are in direct contact with the food, this technology can be termed invasive, which is related to a series of important drawbacks [1], with the most important ones being the large energy consumption and the fact that it cannot be used with solid, prepacked food. It is worth mentioning that however, a few relevant works were published along the years and related to efforts for performing solid food processing and developing noninvasive techniques [2]–[6].

A few years ago, the Plasma and Pulsed Power Group at Loughborough University initiated a research program for the development of a novel, noninvasive PEF technique. In the first phase of this program, conveniently using a very small amount of water of only 4.5 mL, the main results obtained demonstrated that the following conditions hold [1].

Manuscript received October 29, 2021; revised January 29, 2022; accepted April 5, 2022. The review of this article was arranged by Senior Editor J. L. Lopez. *(Corresponding author: Matthew Woodyard.)*

The authors are with the Wolfson School of Mechanical, Electrical and Manufacturing Engineering, Loughborough University, Loughborough LE11 3TU, U.K. (e-mail: m.woodyard@lboro.ac.uk).

Color versions of one or more figures in this article are available at https://doi.org/10.1109/TPS.2022.3167670.

Digital Object Identifier 10.1109/TPS.2022.3167670

1) A noninvasive PEF technique can produce a very significant reduction of bacteria placed in water.

2) Noninvasive PEF systems can produce effects comparable with the standard invasive PEF systems, but using much less energy.

3) When noninvasive PEF experiments are performed, monitoring of the electric field using the Kerr effect in water is essential.

Based on these important findings, it is possible now to think about a noninvasive PEF proof-of-concept system for industrial processing of prepacked food. The packaged food, solid or liquid, would be immersed in a water tank with a pulsed power generator producing a series of very intense PEF impulses in the rather large volume of water containing the food sample to be processed.

This present article is related to the development of the MV-class pulsed power system to generate intense PEFs in a very large volume of water, with the electric field being monitored using a Kerr effect sensor. First, the design of the pulsed power generator and its manufacture will be described. Second, the water tank load, including the Kerr effect sensor, will be introduced. Third, the main results obtained during the first campaign of testing will be presented and discussed. This article will end with conclusions and a brief presentation of the way ahead.

II. Practical Arrangement

The PEF system is made from three parts, as shown in Fig. 1: a pulsed power high voltage (HV) generator, a crowbar switch, and a (water) capacitive load, with the overall equivalent electric scheme shown in Fig. 2. In what follows, the three parts will be presented separately, together with their corresponding diagnostics.

A. Pulsed Power Generator

For an air-core Tesla transformer to operate efficiently, two things are essential: as presented in the following, the natural frequencies of the two winding circuits must be equal and the magnetic coupling coefficient must be: $k = (2n-1)/(2n^2-2n+1)$, where for $n = 1, 2, 3, 4, \ldots$, one obtains $k = 1, 0.6, 0.385, 0.28, \ldots$, As the design of an air-core transformer with a coupling coefficient approaching 1 is

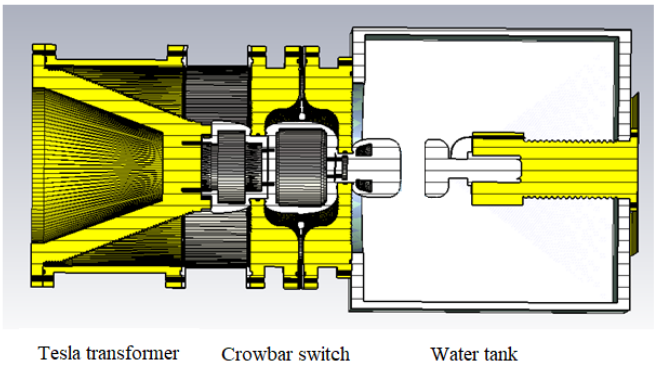

Fig. 1. CAD drawing of the PEF system.

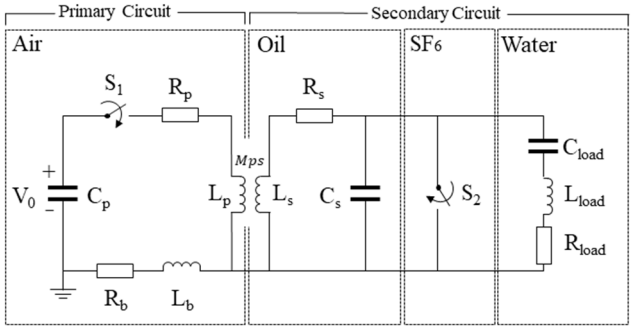

Fig. 2. Equivalent electric scheme of the PEF system based on a Tesla transformer pulsed power generator. See the text for details.

not possible, the next value is usually chosen, i.e., $k = 0.6$. It is worth mentioning the important published works dedicated to the development of such MV-class air-core Tesla transformer-based systems [7]–[9].

The present MV-class generator, with the electrical equivalent scheme presented in Fig. 2, is designed as a dual resonance air-core Tesla unit. The system's architecture is based on the previously reported development of a very successful 0.6 MV Tesla-based generator [10], used for producing 10-GW impulses with a rise time of a few hundreds of picoseconds [11], [12]. Naturally, most of the techniques described in those works were applied in the design of the present system, and therefore, they will not be required to be described here in all details.

The primary circuit of the air-core transformer is operated in air and energized using a capacitor bank containing three parallel-mounted, low-inductance capacitors manufactured by NWL [13], each with a capacitance of 220 nF. The capacitor bank, which can be charged up to an initial voltage of 32 kV, is discharged by a trigatron-type SG-131 BM using pressurized N_2 and triggered with a trigger head pulse transformer-type THD-06 HP that allows operation of the trigatron up to 100 pps. The pulse transformer is controlled by a trigger generator-type PG-103D via a 20-m fiber-optic isolation link. All these components are commercially available from R. E. Beverly III & Associates [14]. The capacitor bank is connected through a very short parallel-plate transmission line to a

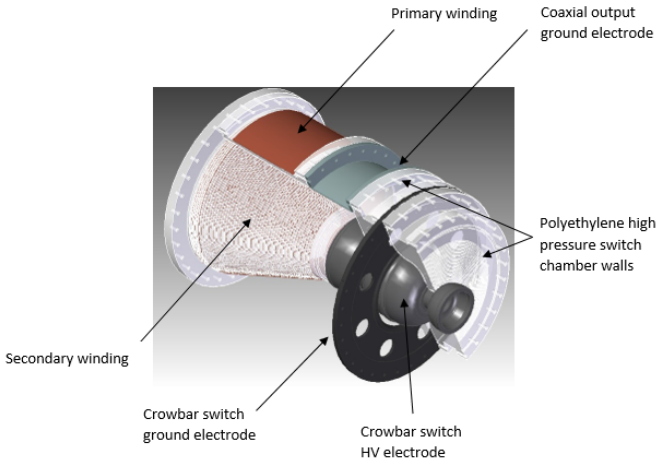

Fig. 3. CAD drawing of the MV-class Tesla transformer.

single-turn primary coil made from a 0.1-mm-thick, 200-mm-wide copper sheet, having an inner diameter of 220 mm.

The transformer secondary helical winding (see Fig. 3) is mounted on a conical plastic former and placed inside an oil tank having the following characteristics: radii along the plastic conical former, maximum 200 mm and minimum 96 mm, axial length of 300 mm, and a total number of 50 turns of round insulated conductor diameter of outer diameter 3.17 mm with a copper core of 1.5 mm diameter are mounted in a helical groove in the plastic former with an axial pitch of 6 mm; the first five turns of the secondary winding have all the same maximum 200 mm outer radius.

The secondary winding is coupled to a central HV electrode, attached to the corresponding HV electrode of the crowbar switch using the multilam technology [15]. The central HV electrode forms a coaxial output (see Fig. 3) with a surrounding aluminum cylindrical ground electrode, 400 mm inner diameter, into which a V-dot sensor (described below) is mounted.

The dual resonance Tesla transformer generates a negative polarity secondary voltage peak, as required by the design of the crowbar switch.

B. MV-Class Crowbar Switch

The crowbar switch assembly is composed of the following components (see Figs. 3 and 4):

1) connector to the HV output of the transformer;
2) central HV cylindrical electrode;
3) connector to the HV water electrode;
4) ground disk electrode;
5) high-pressure SF_6 chamber made from two pieces of polyethylene.

During operation, the chamber is filled with SF_6 according to its characteristic voltage–pressure characteristics (Fig. 5): 4 bar for 0.4 MV and 11 bar for a voltage of 0.9 MV. To avoid an electrical breakdown along the internal parts of the chamber's insulators, the design was based on techniques detailed elsewhere [16]–[18].

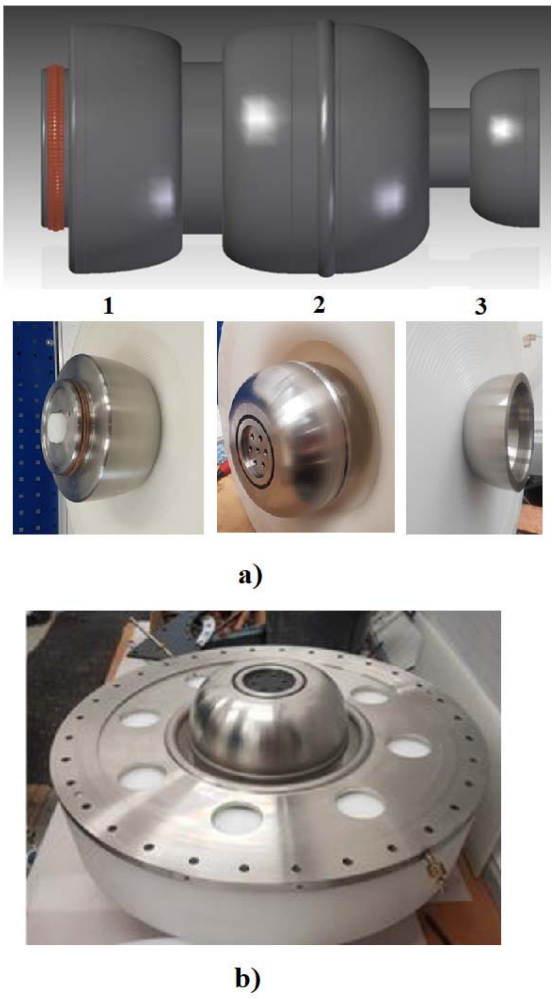

Fig. 4. MV-class crowbar switch. (a) CAD drawing and real components of the HV central electrode assembly. 1—connection to the HV transformer output. 2—MV switch. 3—connection to the HV water electrode. (b) Real components of the MV switch, partly assembled.

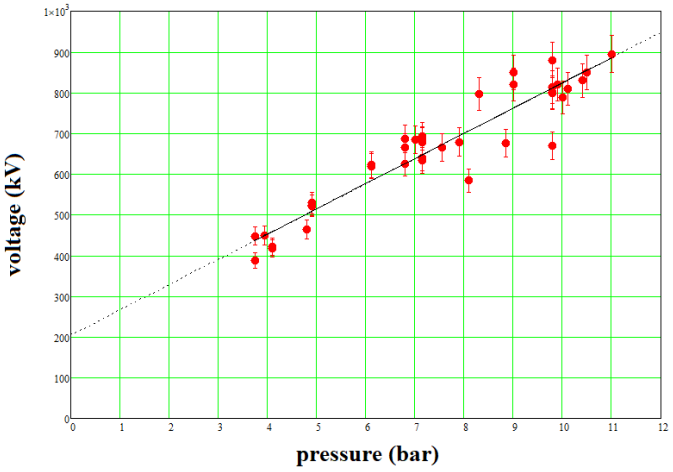

Fig. 5. Crowbar switch voltage–pressure characteristics.

C. Water Tank and Capacitive Load

Two very different water tanks can be used with the pulsed power generator (see Fig. 6): a metallic cylindrical tank that

Fig. 6. MV-class PEF system using (a) plastic water tank and (b) metallic tank.

can be filled with water or oil for various experiments related to testing insulator breakdown phenomena under high electric field stress loading and a plastic cubical-shaped water tank for preliminary proof of concept noninvasive prepacked food processing. In both cases, two stainless steel electrodes are mounted inside, forming an HV water-filled load capacitor. In the case of the plastic tank, the ground electrode is connected through a resistive helical coil to the return ground conductor of the secondary winding of the Tesla transformer. The resistive helical coil is made from four parallel-connected steel wires 0.2 mm in diameter, mounted on a 40-mm outer diameter plastic mandrel and having seven turns with a pitch of 20 mm. The resistive helical coil, by absorbing Joule energy, is damping the oscillatory current generated after the crowbar action, thus protecting the crowbar switch from overheating and at the same time reducing the intensity of the shock wave pressure generated in the gas chamber by its plasma channel.

The two tanks are usually operated at a temperature around 21 °C, using deionized water having a resistivity better than 5 MΩ · cm. Both water tanks have mounted a pair of optical windows allowing the laser beam used in the Kerr effect sensor

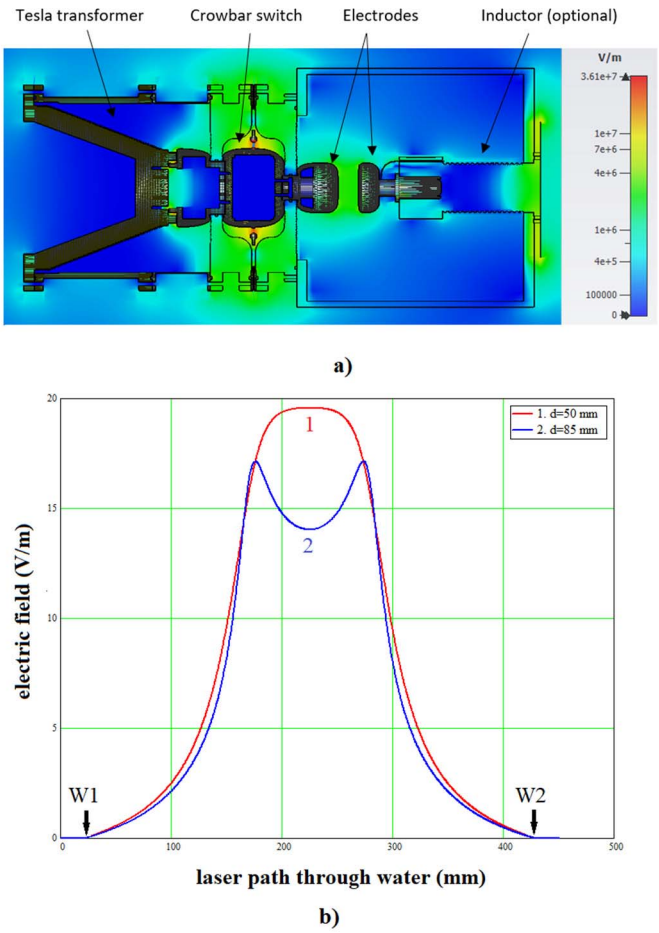

Fig. 7. Electrostatic field inside the system (a) overall 3-D electric field distribution and (b) electric field distribution along the laser beam in the metallic water tank for 1 V applied across electrodes, as required for calculating the integral in (1). Two cases are presented as lines 1 and 2: line 1. For an interelectrode distance $d = 50$ mm and the laser beam at 25 mm from the HV electrode, the field is homogeneous having a "plateau" line 2. For $d = 85$ mm and the laser beam at 10 mm from the HV electrode, due to the proximity, the field is inhomogeneous with a double peak. W stays stands for optical windows (see Fig. 8).

to pass through the water on a path situated between the two electrodes and parallel to their adjacent surfaces.

D. Numerical Modeling

Various numerical techniques, using corresponding software, were applied for the design of the pulsed power generator: filamentary modeling was implemented using MATHCAD [19], a circuit solver using PSpice [20], and an electrostatic solver using CST Studio Suite [21]. With reference to Fig. 2, the complete set of parameters of the pulsed power generator and its load have been first calculated (or estimated) and later confirmed during preliminary experimentation.

Primary Circuit:

Capacitance: $C_p = 660$ nF.

Charging voltage: $V_0 = 10$–32 kV.

Self-inductance: $L_b = 46.6$ nH.

Resistance: $R_b = 23.3$ mΩ.

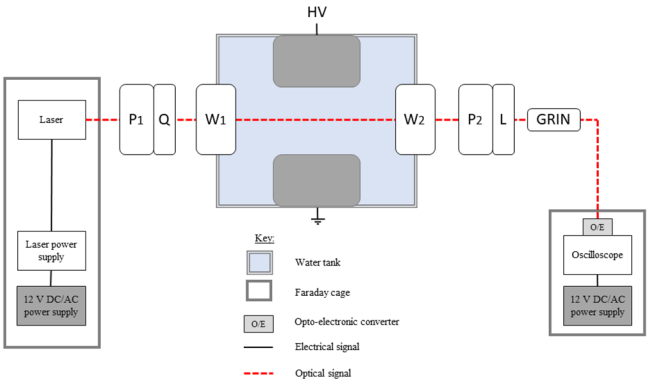

Fig. 8. Schematic of the optical arrangement for the Kerr effect in water. P is for polarizers, Q is for a quarter-wave plate, W is for optical windows, L is for a focus lens, and GRIN is for a gradient index collimator pigtailed on a fiber-optic connected to an optoelectronic converter OE attached to an oscilloscope.

HV Transformer:

Primary winding self-inductance: $L_p = 480$ nH.

Primary winding resistance: $R_p \approx 1.1$ mΩ.

Mutual inductance: $M_{\text{ps}} = 8.7$ μH.

Secondary winding self-inductance: $L_s = 471$ μH.

Secondary resistance: $R_s = 21$ Ω.

Secondary capacitance: $C_s = 90$ pF.

Magnetic coupling coefficient: $k = (M\text{ps})/((LpLs)^{1/2}) = 0.58$.

Load Circuit:

Load capacitance: $C_{\text{load}} = 530$ pF/580 pF for the plastic/metallic tank, for the same inter-electrode gap $d = 50$ mm.

Load self-inductance (helical coil): $L_{\text{load}} = 16$ μH.

Load resistance (helical coil): $R_{\text{load}} = 18$ Ω.

The natural frequency f of the two circuits of the Tesla transformer is: 1) for the primary winding $f_p = 1/(2\pi((L_b + L_p)C_p)^{1/2}) = 270$ kHz and 2) for the secondary winding $f_s = 1/(2\pi((L_s + L_{\text{Load}})(C_s + C_{\text{Load}}))^{1/2}) = 290$ kHz.

The overall Tesla transformer energy efficiency, defined as $\gamma = (C_s + C_{\text{load}})V_{\text{max}}^2/C_p V_0^2$, has a value close to 85% for the plastic tank and close to 92% for the metal tank, in both cases for a charging voltage of $V_0 = 30$ kV and for a corresponding output voltage of $V_{\text{max}} = 0.9$ MV.

E. Diagnostics

The charging voltage across the primary winding circuit capacitor bank is monitored with a resistive divider, while an I-dot probe mounted in a tunnel built in the parallel transmission line is used to measure the primary discharge current.

As already mentioned, a V-dot probe operated under oil is mounted inside the coaxial output of the transformer secondary winding. A second V-dot probe, operated under water, is mounted in the water tank, just above the HV electrode. Both V-dot probes are using a design already presented in [10].

The electric field distribution generated inside the water tank when the HV electrode is energized by the MV transformer is

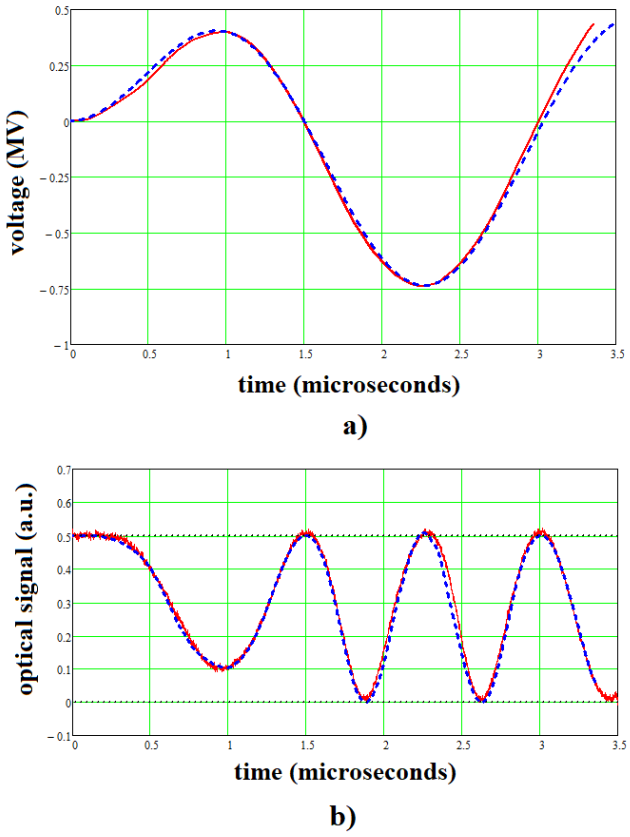

Fig. 9. Results from a test without crowbar, with the plastic tank having an interelectrode distance of 50 mm. Red full lines represent experimental data. The blue dotted lines represent (a) theoretical prediction provided by the Tesla transformer filamentary model and (b) light signal calculated with (1) using the experimental voltage signal.

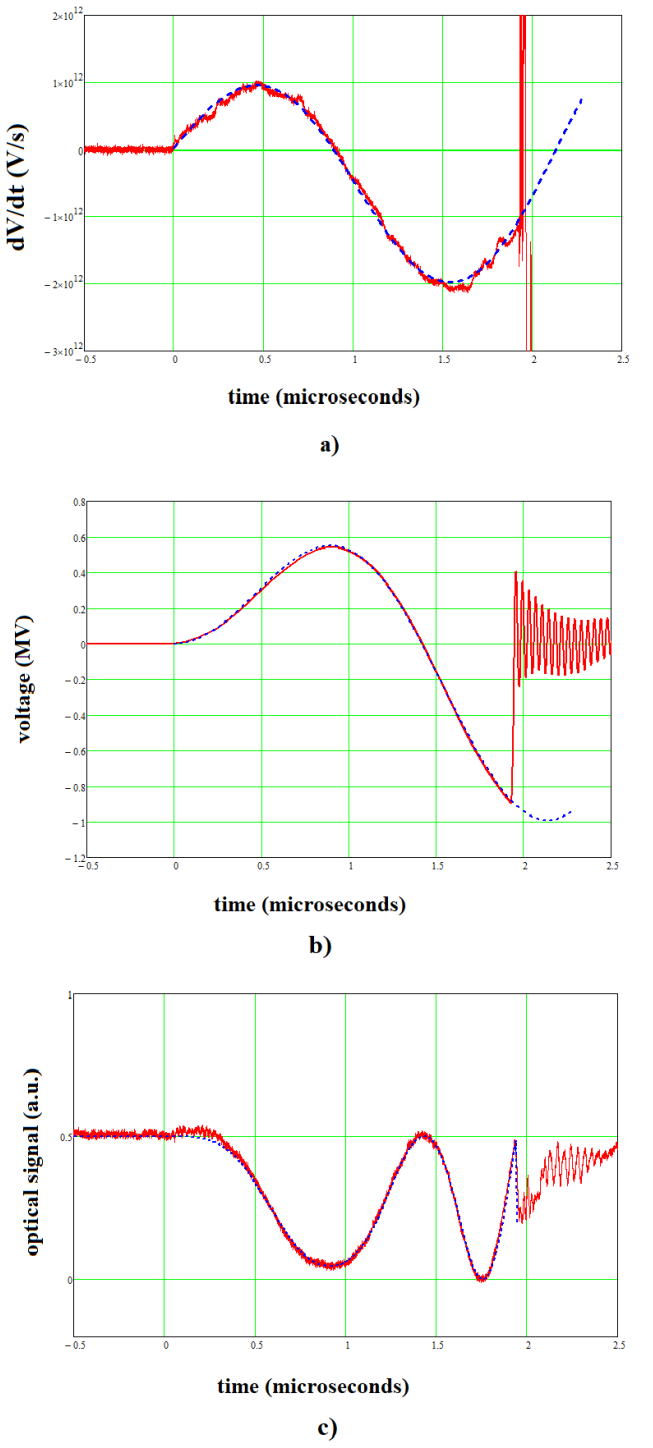

Fig. 10. Results from a test with the metal tank and interelectrode distance 50 mm. Red full lines represent experimental data. The blue dotted lines represent: (a) theoretical predictions for the time rate of change of voltage applied on the water capacitor provided by the Tesla transformer filamentary model, (b) voltage applied on the water capacitor, and (c) Kerr light signal calculated with (1) using the experimental voltage signal.

calculated using a CST electrostatic solver. A typical result is shown in Fig. 7(a). However, the fact the transformer output voltage impulses during the MV tests are accurately measured by a V-dot probe and that a CST model calculates the corresponding electric fields is not a guarantee that those electric fields are indeed produced inside the water tank. For example, currents could flow through the water, dramatically changing the electric field distribution, local plasma streamers can affect the field strength, and so on. The only way to trust the electric field distribution calculated by CST is to directly measure the electric field along a laser path using the Kerr effect in water. The present Kerr effect sensor uses techniques already described in great detail elsewhere [22], [23]. The schematic of the optical arrangement is presented in Fig. 8. The time-varying optical output $I(t)$ detected by the optoelectronic converter (having a bandwidth of 0.85 GHz) is given by Malus' law [23]:

$$I(t) = I_{\max} \sin^2\left(\pi B \int_0^l E(x,t)^2 dx - \frac{\pi}{4}\right) \qquad (1)$$

where $I_{\max}$ is the maximum light intensity and $B = 2.746 \times 10^{-14}$ rad·m/V^2 is the Kerr constant for water [15]. $E(x,t) = V(t)f(x)$ is the time-varying electric field distribution, where $V(t)$ is the voltage impulse applied to the electrodes and $f(x)$ represents the field distribution, for 1 V applied across the electrodes, along the laser path (a straight line) shown in Fig. 7(b). The field integral $\int_0^l f(x)^2 dx$ is performed along the laser path, from $x = 0$ to $x = l$ with $l = 500$ mm,

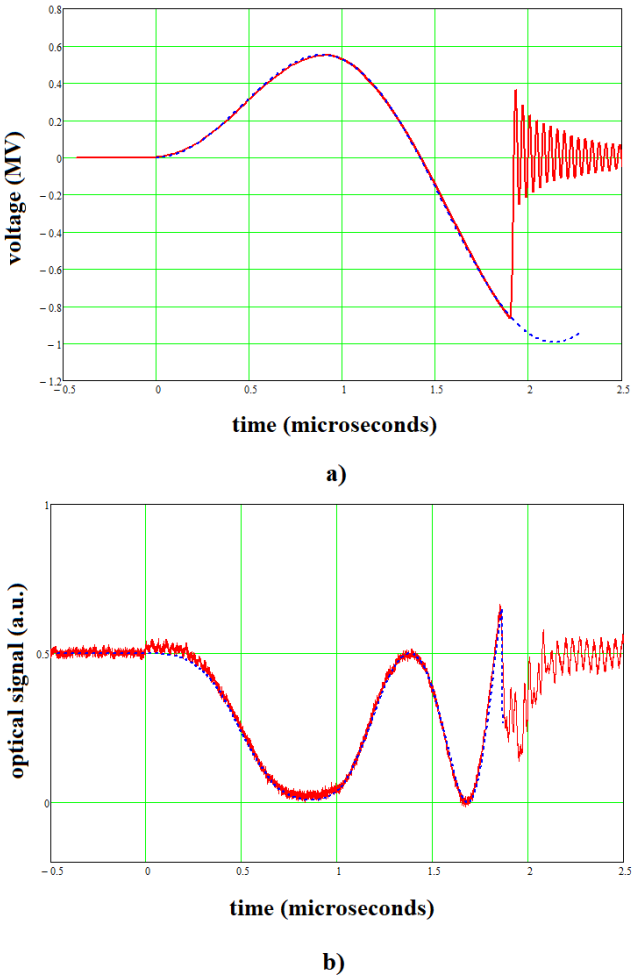

Fig. 11. Results from a test with the metal tank and interelectrode distance 85 mm. Red full lines represent experimental data. The blue dotted lines represent: (a) theoretical prediction of the voltage applied on the water capacitor provided by the Tesla transformer filamentary model and (b) Kerr light signal calculated with (1) using the experimental voltage signal.

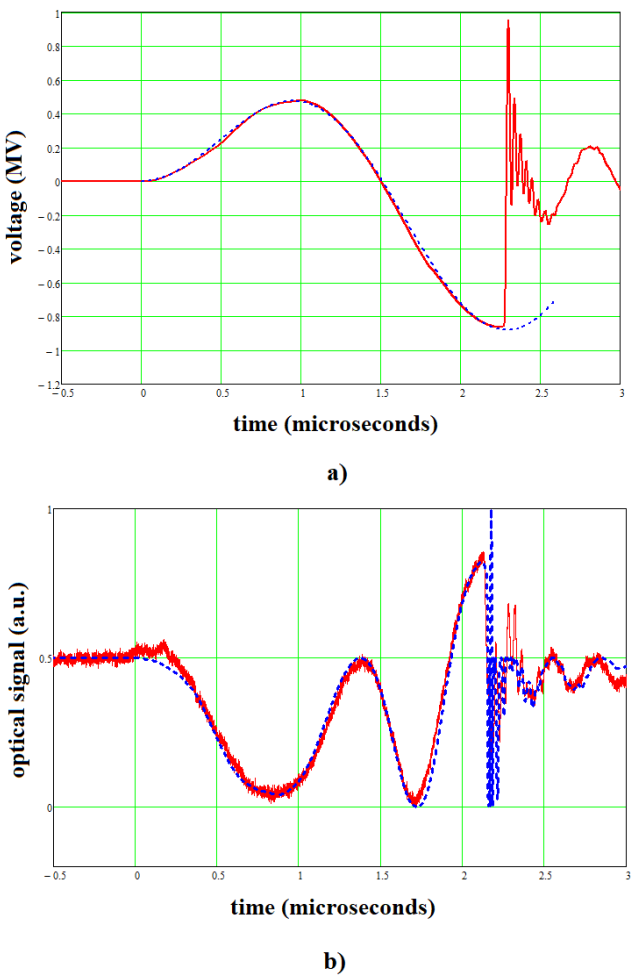

Fig. 12. Results from a test with the plastic tank and interelectrode distance of 50 mm. Red lines represent the experimental data. The blue dotted lines represent (a) theoretical prediction of the voltage applied on the water capacitor provided by the Tesla transformer filamentary model and (b) Kerr light signal calculated with (1) using the experimental voltage signal.

as shown in Fig. 7(b). The $-\pi/4$ term is because of a quarter-wave plate used in the present optical arrangement to enhance the precision of the measurement [23].

The following procedure is used to enable benchmarking the CST predictions for an experiment.

1) An optical output $I_{\text{exp}}(t)$ is recorded experimentally; this is purely the result of an optoelectronic phenomenon.
2) The voltage impulse $V(t)$ is measured using the calibrated V-dot probe.
3) The CST provides the field integral $\int_0^l f(x)^2 dx$ (a constant), calculated for 1 V applied on the HV electrode of the water capacitor.
4) By introducing both $V(t)$ and the value of the electric field integral in (1), an optical output can be estimated as $I_{\text{est}}(t)$.
5) By successfully comparing $I_{\text{exp}}(t)$ with $I_{\text{est}}(t)$, the electric field distribution provided by CST is thus benchmarked.

III. Experimental Results

A. Experiments Without Crowbar Switch

For food processing applications, as well as electric breakdown studies, it is useful to be able to generate long-duration electric fields. Fig. 9 shows the typical results obtained from a test using the plastic tank with a peak voltage close to 0.75 MV. During such a test, the electrostatic energy, which is initially stored in the primary winding circuit capacitor (C_P in Fig. 2), is transferred to the water load (C_S in Fig. 2) and back many times. However, this process produces reversed polarity charging of the capacitor bank and this in turn can generate dangerous accelerating aging of the capacitors. Therefore, such tests were limited to a charging voltage of about 24 kV.

B. Experiments With Crowbar Switch and Metallic Tank

Fig. 10 presents the main results obtained from a typical test with the metallic tank, with the capacitor bank charged to 30 kV and the water capacitor electrodes separated at 50 mm.

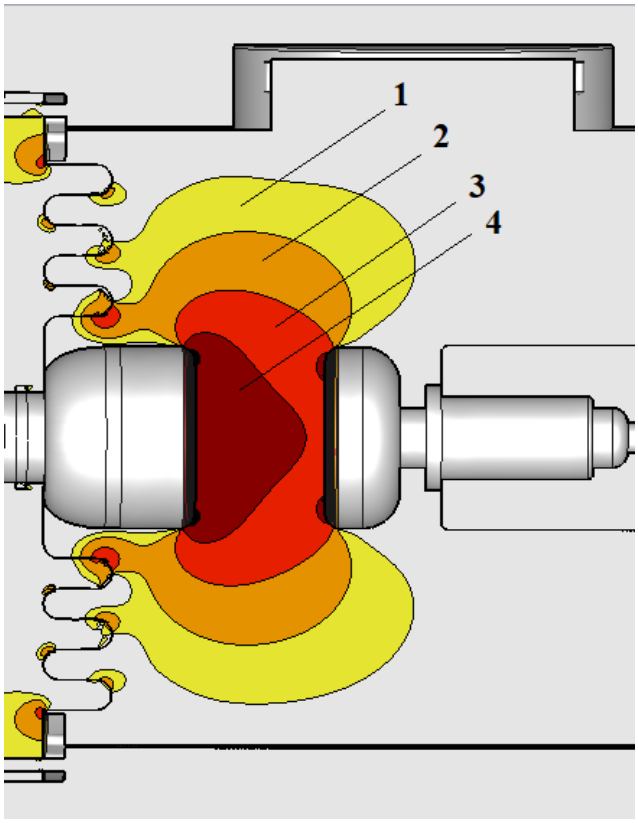

Fig. 13. Shape of the water volumes inside the metal tank corresponding to the PEFs strengths indicated in the following, for an interelectrode distance of 85 mm: 1) from 10 kV/cm up to 50 kV/cm; 2) from 50 kV/cm up to 75 kV/cm; 3) from 75 kV/cm up to 100 kV/cm; and 4) 100 kV/cm and higher.

The time rate-of-change *dV/dt* and the voltage generated [red lines in Fig. 10(a) and (b)] are both very close to the predictions obtained from the Tesla transformer filamentary model. The laser used in the Kerr effect measurement is installed such that the beam is parallel to and at 25-mm distance from the surface of the HV electrode. The predictions of (1) using the voltage impulse measured by the V-dot probe [blue dotted line in Fig. 10(c)] are very close to the optical signal detected during the test. The very good fit indicates that the electric field distribution predicted by the CST is correct.

Fig. 11 presents the results with the capacitor bank charged to 30 kV and the electrodes separated at 85 mm with the laser beam at 10 mm from the surface of the HV electrode. Again, both the predictions made by the Tesla filamentary model and those obtained using (1) and the experimental voltage signal are close to the experimental data.

C. Experiments With Crowbar and Plastic Tank

Fig. 12 presents the results with the capacitor bank charged to 30 kV with the electrodes separated at 50 mm and the laser beam at 25 mm from the surface of the HV electrode. In this test, to minimize the shock waves generated by the crowbar, the supplementary resistive helical coil described earlier is mounted inside the water tank. Like before, all theoretical predictions are close to the data obtained during testing close to the data obtained during testing.

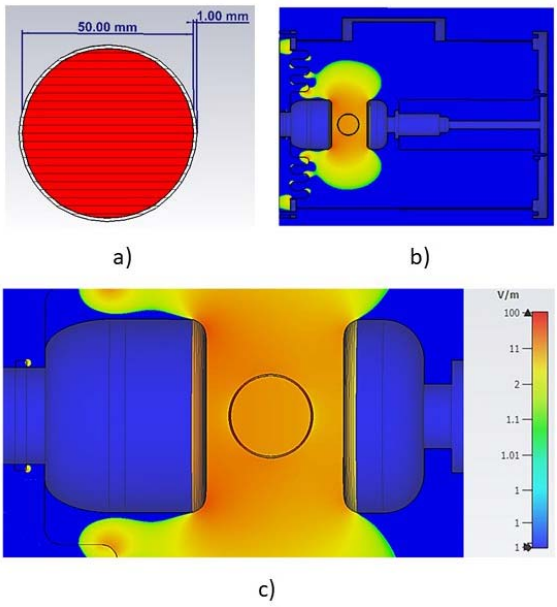

Fig. 14. CST predictions of the electric field distribution during a contactless processing of a prepacked food for a 1 V applied on the HV electrode. (a) Spherical food sample covered with a 1-mm layer of plastic. (b) Overview of the electric field distribution inside the metal water tank. (c) Detail showing the electric field inside the food being processed.

D. Volumes Under Intense PEF

The experimental results successfully benchmarked the CST calculation, allowing the correct estimation of the volumes under various PEF intensity loading. Fig. 13 shows an example of the shape of these volumes calculated by the CST software and Table I presents a summary of the main results.

E. Comments Related to Experimental Results

The plastic tank is providing better results, with slightly larger volumes being stressed by the same electric field strength as in the metal tank. Related to this, if we compare the results in Fig. 10 (metal tank) with those shown in Fig. 12 (plastic tank), we clearly note the increased modulation of the Kerr effect signal for the tests performed in the plastic tank. We also note the high-frequency oscillations in Fig. 10, after the HV switch action, compared with the low-frequency oscillations of the interelectrode voltage in Fig. 12. This difference could play a role when food processing will be attempted.

F. CST Prediction of the Electric Field Distribution During a Possible Contactless Prepacked Food Processing

For simplicity, in the theoretical prediction considered here, the food has a spherical shape, covered with a layer of 1-mm-thick plastic [see Fig. 14(a)]. The frequency-dependent model for the relative permittivity of the food sample considered in the CST calculations is for poultry, as provided in [24]. The plastic packaging is made of polyimide with a relative permittivity of 3.5. The very thin layer of plastic requires an extremely demanding numerical computation, with almost two billion finite elements being used in the CST model. The

TABLE I
VOLUMES IN LITERS CORRESPONDING TO VARIOUS PEFs STRENGTH IN kV/cm FOR THE TWO TANKS AND FOR 50 mm AND 85 mm INTERELECTRODE DISTANCE

Metal tank		>50kV/cm	>75kV/cm	>100kV/cm
	50mm	1.79 L	1.16 L	0.88 L
	85mm	2.11 L	1.30 L	0.65 L
Plastic tank		>50kV/cm	>75kV/cm	>100kV/cm
	50mm	1.81 L	1.18 L	0.91 L
	85mm	2.19 L	1.33 L	0.80 L

results of the calculations, for the HV electrode charged to 1 V, are presented in Fig. 14(b) and (c). The results demonstrate that when the system is operated between 0.5 and 1 MV, the average electric field inside the food is between 50 kV/cm and 100 kV, while the electric field stressing the plastic packaging has peak values between 70 and 140 kV/cm well below the characteristic breakdown field of polyimide.

IV. CONCLUSION AND THE WAY AHEAD

A MV-class pulsed power system capable of generating an intense PEF in large volumes of water have been designed, manufactured, and preliminarily tested. During the first experimental campaign, the system demonstrated that it could produce electric fields of the order of 100 kV/cm in a volume approaching 1 L of water.

Plans for future include the noninvasive (contactless) processing of prepacked solid food samples, as well as various electric breakdown tests using various dielectric materials.

REFERENCES

[1] B. M. Novac *et al.*, "Demonstration of a novel pulsed electric field technique generating neither conduction currents nor Joule effects," *IEEE Trans. Plasma Sci.*, vol. 42, no. 1, pp. 216–228, Jan. 2014.

[2] B. Mazurek, P. Lubicki, and Z. Staroniewicz, "Effect of short HV pulses on bacteria and fungi," *IEEE Trans. Dielectr. Electr. Insul.*, vol. 2, no. 3, pp. 418–425, Jun. 1995.

[3] D. J. Bolton, T. Catarame, C. Byrne, J. J. Sheridan, D. A. McDowell, and I. S. Blair, "The ineffectiveness of organic acids, freezing and pulsed electric fields to control *Escherichia coli* O_{157}: H_7 in beef burgers," *Lett. Appl. Microbiol.*, vol. 34, no. 2, pp. 139–143, Feb. 2002.

[4] B. Roodenburg, S. De Haan, J. A. Ferreira, P. Coronel, P. C. Wouters, and V. Hatt, "Toward 6 $\log_{10}$ pulsed electric field inactivation with conductive plastic packaging material," *J. Food Process Eng.*, vol. 36, pp. 77–86, Feb. 2013.

[5] K. Nowosad, M. Sujka, U. Pankiewicz, and R. Kowalski, "The application of PEF technology in food processing and human nutrition," *J. Food Sci. Technol.*, vol. 58, no. 2, pp. 397–411, Feb. 2021.

[6] L. Astráin-Redín, J. Raso, G. Cebrián, and I. Álvarez, "Potential of pulsed electric fields for the preparation of Spanish dry-cured sausages," *Sci. Rep.*, vol. 9, no. 1, p. 16042, Dec. 2019.

[7] C. E. Baum *et al.*, "JOLT: A highly directive, very intensive, impulse-like radiator," *Proc. IEEE*, vol. 92, no. 7, pp. 1096–1109, Jul. 2004.

[8] E. A. Abramyan, "Transformer type accelerators for intense electron beams," *IEEE Trans. Nucl. Sci.*, vol. NS-18, no. 3, pp. 447–455, Jun. 1971.

[9] G. J. Rohwein, "A three megavolt transformer for PFL pulse charging," *IEEE Trans. Nucl. Sci.*, vol. NS-26, no. 3, pp. 4211–4213, Jun. 1979.

[10] B. M. Novac, M. Wang, I. R. Smith, and P. Senior, "A 10 GW Tesla-driven Blumlein pulsed power generator," *IEEE Trans. Plasma Sci.*, vol. 42, no. 10, pp. 2876–2885, Oct. 2014. [Online]. Available: https://www.mathcad.com/en/try-and-buy/free-trial

[11] M. Wang, B. M. Novac, L. Pécastaing, and I. R. Smith, "Bipolar modulation of the output of a 10-GW pulsed power generator," *IEEE Trans. Plasma Sci.*, vol. 44, no. 10, pp. 1971–1977, Oct. 2016.

[12] B. M. Novac, R. Xiao, P. Senior, L. Pecastaing, and I. R. Smith, "Generation of intense PEFs using a prolate spheroidal reflector attached to the bipolar former of a 10-GW pulsed power generator," *IEEE Trans. Plasma Sci.*, vol. 46, no. 10, pp. 3547–3551, Oct. 2018.

[13] *NWL Products*. Accessed: 2021. [Online]. Available: https://www.nwl.com/products/

[14] *R. E. Beverly III & Associate Products*. Accessed: 2021. [Online]. Available: http://www.reb3.com/products.php

[15] *Staubli Multilam Technology*. Accessed: 2021. [Online]. Available: https://www.staubli.com/en/electrical-connectors/multilam-technology/

[16] T. Yamashita *et al.*, "Estimation of surface breakdown voltage of solid/gas composite insulation with embedded electrode," *IEEE Trans. Dielectr. Electr. Insul.*, vol. 23, no. 5, pp. 3026–3033, Oct. 2016.

[17] A. Pedersen, T. Christen, A. Blaszczyk, and H. Boehme, "Streamer inception and propagation models for designing air insulated power devices," in *Proc. IEEE Conf. Electr. Insul. Dielectric Phenomena*, Virginia Beach, VA, USA, Aug. 2009, pp. 604–607.

[18] N. L. Allen and P. N. Mikropoulos, "Streamer propagation along insulating surfaces," *IEEE Trans. Dielectrics Electr. Insul.*, vol. 6, no. 3, pp. 357–362, Jun. 1999.

[19] *PTC Mathcad*. Accessed: 2021. [Online]. Available: https://www.mathcad.com/en/whats-new

[20] *Cadence Products*. Accessed: 2021. [Online]. Available: http://www.cadence.com/products/orcad/pspice_simulation/pages/defaultaspx

[21] *CST Products*. Accessed: 2021. [Online]. Available: https://www.cst.com/Products

[22] B. M. Novac *et al.*, "Determination of the Kerr constant of water at 658 nm for pulsed intense electric fields," *IEEE Trans. Plasma Sci.*, vol. 40, no. 10, pp. 2480–2490, Oct. 2012.

[23] B. M. Novac *et al.*, "Temperature dependence of Kerr constant for water at 658 nm and for pulsed intense electric fields," *IEEE Trans. Plasma Sci.*, vol. 44, no. 6, pp. 963–967, Jun. 2016.

[24] H. Zhuang, S. O. Nelson, S. Trabelsi, and E. M. Savage, "Dielectric properties of uncooked chicken breast muscles from ten to one thousand eight hundred megahertz," *Poult Sci.*, vol. 86, no. 11, pp. 2433–2440, 2007.

Matthew Woodyard (Graduate Student Member, IEEE) received the B.Eng. degree (Hons.) from Loughborough University, Loughborough, U.K., in 2015, where he is currently pursuing the Ph.D. degree with the Plasma and Pulsed Power Group under the supervision of Prof. B. M. Novac.

His research interests include Tesla transformer driven pulsed power generation, large-volume intense pulsed electric field (PEF) applications in water, low-frequency magnetic field penetration of thick metallic shields, novel high-voltage (HV) switch design, and 3-D electromagnetic modeling of pulsed power systems.

Mr. Woodyard is a Student Member of the International Society of Pulsed Power (ISP). He was a recipient of the EAPPC Outstanding Young Researcher Award in 2021.

Bucur M. Novac (Senior Member, IEEE) received the M.Sc. and Ph.D. degrees from the University of Bucharest, Bucharest, Romania, in 1977 and 1989, respectively.

He joined Loughborough University, Loughborough, U.K., in 1998, where he is currently a Professor of pulsed power. His research interests include compact and repetitive high-power systems, explosively and electromagnetically driven magnetic flux compression generators and their applications, electromagnetic launchers, ultrafast magneto and electrooptic sensors, and 2-D modeling of pulsed-power systems. He has coauthored two books on explosive pulsed power and has published more than 200 refereed papers and conference contributions.

Prof. Novac is a Voting Member of the Pulsed Power Science and Technology Committee in the IEEE Nuclear and Plasma Science Society. He is also a member of the International Steering Committees for the MEGAGAUSS conferences and the Euro-Asian Pulsed Power conferences. He is also a member of the organizing committee of the IEEE International Power Modulator and High Voltage (HV) Conference and Co-Chaired the U.K. Pulsed Power Symposium. He is a Chartered Engineer and a fellow of The Institution of Engineering and Technology (IET), U.K.

Peter Senior (Member, IEEE) received the Honors degree in physics with electronics from the University of Leicester, Leicester, U.K., in 1977.

He began his career at the Department of Electronic and Electrical Engineering, Loughborough University, Loughborough, U.K., researching ultrasonic nondestructive evaluation, extending into nonlinear (finite amplitude) acoustics. He was one of the founding members of the Pulsed Power Research Group. He has worked on propellant and explosive pulsed MHD generators and also produced systems to support a Flux Compressor Program. His other work has included high-efficiency launchers and the electromagnetic protection of armored vehicles. He has produced a number of transportable high energy, high power systems, varying in size between fitting into a van, and up to two ISO containers, supplied by diesel generators. This has required expertise in the health and safety aspects of integrating pulsed power systems with the equipment of sponsoring and collaborating bodies.

Mr. Senior is a member of the Institute of Physics and a Chartered Physicist.

Jessica M. Stobbs (Graduate Student Member, IEEE) received the M.Sc. degree in physics from Loughborough University, Loughborough, U.K., in 2018, where she is currently pursuing the Ph.D. degree under the supervision of B. M. Novac with the Plasma and Pulsed Power Group.

Her research uses a combination of electrical, acoustic, and optical diagnostics to study nanosecond electrical breakdown of water for generating ultrasound.